A wide range kinetic modeling study of pyrolysis and oxidation of methyl butanoate and methyl decanoate. Note I: Lumped kinetic model of methyl butanoate and small methyl esters

ARTICLE *in* ENERGY · JULY 2012

Impact Factor: 4.84 · DOI: 10.1016/j.energy.2012.01.044

Energy 43 (2012) 124–139

Contents lists available at SciVerse ScienceDirect

Energy

journal homepage: www.elsevier.com/locate/energy

A wide range kinetic modeling study of pyrolysis and oxidation of methyl butanoate and methyl decanoate. Note I: Lumped kinetic model of methyl butanoate and small methyl esters

Roberto Grana, Alessio Frassoldati, Alberto Cuoci, Tiziano Faravelli, Eliseo Ranzi*

Dipartimento di Chimica, Materiali e Ingegneria Chimica "G.Natta", Politecnico di Milano, Piazza Leonardo da Vinci 32, 20133 Milano, Italy

ARTICLE INFO

Article history:
Received 30 August 2011
Received in revised form
12 January 2012
Accepted 18 January 2012
Available online 25 February 2012

Keywords:
Methyl esters
Biodiesel
Methyl butanoate
Detailed kinetics
Lumped models
Low temperature oxidation

ABSTRACT

A lumped kinetic model of methyl butanoate pyrolysis and oxidation is presented and discussed in this work. The hierarchical approach first required the development and validation of sub-mechanisms of small esters such as methyl formate, methyl acrylate and methyl crotonate. A broad-ranging validation of the whole kinetic scheme of methyl butanoate oxidation was then carried out through comparisons with experimental data obtained in shock tube devices, plug flow and jet stirred reactors, rapid compression machines and premixed laminar flames. A detailed analysis of laminar flame speeds complements and extends this kinetic study. The lumped model predicts a wide range of experiments well, thus constituting a flexible and reliable kinetic scheme despite the reduced number of species involved. Moreover, this lumped approach and the proposed model lay the foundation for an extension to biodiesel fuel modeling.

1. Introduction

Biodiesels are complex mixtures of multi-component alkyl esters of long-chain fatty acids, generally produced by transesterification of soy and rapeseed oil with methanol. These biofuels are mostly composed of unsaturated methyl esters, methyl oleate ($C_{19}H_{36}O_2$) and methyl linoleate ($C_{19}H_{34}O_2$), with minor quantities of saturated components such as methyl palmitate ($C_{17}H_{34}O_2$) and methyl stearate ($C_{19}H_{38}O_2$). Significant amounts of methyl linolenate ($C_{19}H_{32}O_2$), characterized by three double bonds, are also present [1]. Knothe [2] provides a general and comparative discussion of aspects such as fuel production and energy balance, fuel properties, environmental effects including exhaust emissions and co-products. Pitz and Mueller [3], in a recent review on the progress in the development of diesel surrogate fuels, systematically collected and revised the available literature on methyl esters present in biodiesel also. The large number of recent papers on these topics confirms the great interest in this research area [4–13]. Since the pioneering work on methyl butanoate of Fisher et al. [14], several combined efforts regarding the detailed kinetic modeling of fatty acid methyl esters (FAME) were carried out by the research teams from Galway [15–18], Lawrence Livermore National Laboratory [1,19–22], Nancy [23–31], Orleans [32–39], and Princeton [40–42]. As a result of these and other experimental and kinetic modeling activities, there are now several experimental measurements obtained with different devices and in different laboratories, and relating to various fuels. At the same time, there is also a significant understanding of the intrinsic kinetics and reaction classes of pyrolysis and oxidation of methyl esters.

The detailed kinetic schemes developed, validated, and available in the literature are constituted by a very large number of species and reactions. The methyl decanoate mechanism developed by Herbinet et al. is made up of 3012 species and includes 8820 reactions [1]. The recent, excellent kinetic modeling study by Westbrook et al. [22] reports a very detailed kinetic scheme for the five major components of soy biodiesel and rapeseed biodiesel fuels: methyl stearate, methyl oleate, methyl linoleate, methyl linolenate, and methyl palmitate. The resulting reaction mechanism contains more than 4800 chemical species and nearly 20,000 elementary chemical reactions. These large numbers of reactions and species are the result of the lack of symmetry of the methyl ester molecules and of the numerous types of reactions taken into account. These dimensions often limit the possibility of a complete validation of the mechanisms as well as their direct applicability. Several different reduction and simplification techniques, including

* Corresponding author.
E-mail address: eliseo.ranzi@polimi.it (E. Ranzi).

0360-5442/$ – see front matter © 2012 Elsevier Ltd. All rights reserved.
doi:10.1016/j.energy.2012.01.044

chemical lumping, are thus applied to make the use of these large kinetic schemes viable for practical applications [43]. Since it was not possible to use the detailed mechanism of methyl decanoate [1] to simulate the counterflow flames because of the number of species and reactions involved, Seshadri et al. [44] reduced the detailed mechanism using the 'directed relation graph' method and obtained a skeletal mechanism of 125 species involved in 713 elementary reactions. Critical conditions of extinction and ignition were thus calculated and compared with experimental data. Similarly, Luo et al. [45] derived a skeletal mechanism with 118 species and 837 reactions from the same mechanism by using an improved version of the DRG method.

Based on these premises, the present work aims to develop and validate a general lumped kinetic model capable of characterizing the decomposition and oxidation behavior of the different methyl esters and biofuels in a wide range of operating conditions. This work will first benefit from all the recent kinetic research on ester fuels, and will also take advantage of all the previous experience in lumped kinetic modeling of large alkanes, cycloalkanes, and alkenes [46–49].

This kinetic work refers to the low and high temperature kinetic model of pyrolysis and combustion of methyl esters up to methyl decanoate. A relevant aspect of the proposed biofuel sub-model is that it only requires the addition of a limited number of new molecules and radicals to extend the previous general kinetic model to biofuel combustion. On this basis, a more flexible and general validation of the model can be applied in a wider range of experimental conditions.

2. Development and validation of the lumped kinetic model

This work is organized into two separate notes for convenience sake. Due to the hierarchical and modular approach used in the development and validation of the kinetic schemes, Note I of this paper first analyses experimental data on the oxidation of methyl formate (MF), methyl acrylate (MA) and methyl crotonate (MC), and only then discusses the kinetic mechanism of methyl butanoate (MB). Fig. 1 shows the structures and the bond dissociation energies of the four methyl esters.

As already mentioned, the development of the lumped kinetic model takes advantage and relies on the available kinetic experiences on ester fuels. The validation work is discussed sequentially starting with methyl formate. MF is analyzed on the basis of plug flow, shock tube, and low pressure premixed laminar flame experiments. MA and MC are then compared on the basis of shock tube experiments. A wider set of experiments are available for MB oxidation: plug flow, jet stirred, shock tube, rapid compression machine and premixed and diffusion flames. Finally, a comparative discussion of laminar flame speed of small methyl esters will complete this paper.

The extension and validation of the lumped kinetic model to the decomposition and oxidation of methyl esters from methyl butanoate up to methyl decanoate will be the subject of Note II of this work.

3. Methyl formate

Methyl formate (CH_3OCHO) is the simplest methyl ester. Good and Francisco [50] investigated the tropospheric oxidation of methyl formate, using ab-initio techniques. Westbrook et al. [21] developed and validated a first detailed kinetic model for methyl formate combustion in comparison with experiments obtained in fuel rich, low pressure, premixed laminar flames. This mechanism, together with the methyl butanoate mechanism of Fisher et al. [14], provides a first useful guideline of kinetic rules on which to build mechanisms for small and larger esters. The detailed kinetic MF oxidation model discussed and validated by Dooley et al. [41,42] agrees well with different experimental measurements obtained in the Princeton pressurized flow reactor, in the Galway shock tube device, and in low pressure premixed laminar flames.

Methyl formate is mainly converted to methanol and CO, formaldehyde and methane are major intermediate species, while smaller amounts of ethylene and acetylene are also formed, via methyl radical recombination reactions mainly at high temperatures and fuel rich conditions. Molecular reactions play a significant role in methyl formate decomposition. On the basis of an ab-initio kinetic study, Metcalfe et al. [18] analyzed and discussed the following three molecular paths:

$$CH_3OCHO \leftrightarrow CH_3OH + CO \quad (R1)$$

$$CH_3OCHO \leftrightarrow CH_4 + CO_2 \quad (R2)$$

$$CH_3OCHO \leftrightarrow CH_2O + CH_2O \quad (R3)$$

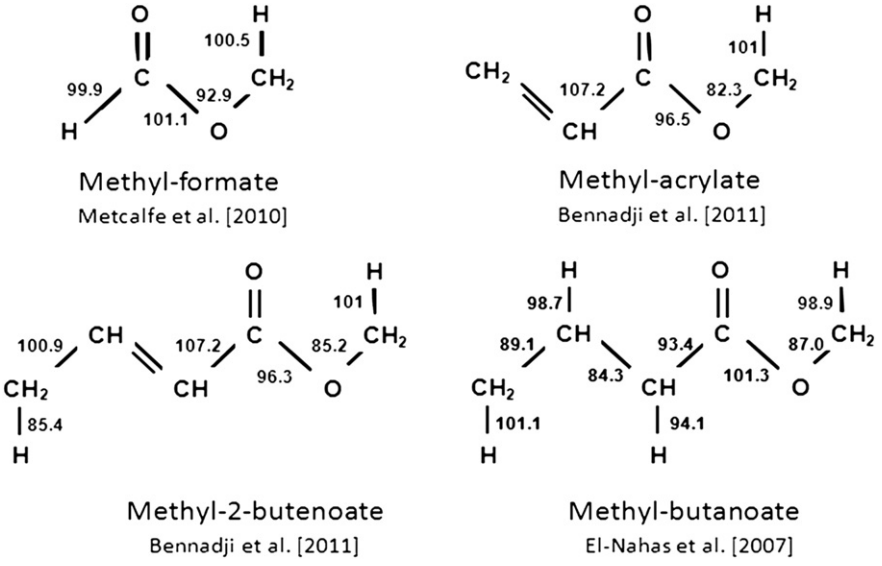

Fig. 1. Structures and bond dissociation energies [kcal/mol] of methyl formate [18], methyl acrylate [28], methyl-2-butenoate [28] and methyl butanoate [15].

According to their conclusions, the MF decomposition is dominated by the channel producing methanol and carbon monoxide at all temperatures and pressures, while the other two channels producing two molecules of formaldehyde, and methane and carbon dioxide can be removed from the kinetic mechanism. Molecular reaction R1 to form CO and methanol was already included in the methyl formate oxidation mechanism presented by Westbrook et al. [21] with a pressure independent rate constant $1.0 \times 10^{14} \exp(-63{,}000/RT)\ s^{-1}$, while the high pressure limit of the same reactions as proposed by Metcalfe et al. [18] is lower: $2.13 \times 10^{12}\ T^{0.735} \exp(-69{,}000/RT)\ s^{-1}$. At 1000 K, the Westbrook estimate is about 5 times larger and this value is closer to the high pressure limit recently proposed by Dooley et al. [41]: $2.0 \times 10^{13} \exp(-60{,}000/RT)\ s^{-1}$. In line with the conclusions and the mechanism of Dooley et al. [42], our kinetic mechanism included not only the molecular reaction to form methanol and carbon monoxide R1, but also R2 to directly form methane and carbon dioxide, and R3 with formaldehyde formation.

A small subset of molecular and radical reactions allows us to extend the previous general kinetic scheme to also describe methyl formate decomposition properly. Initiation reactions are simply obtained via the reverse recombination reactions. These reactions and kinetic parameters are reported in Table 1, together with the primary reactions of pyrolysis and oxidation of methyl acrylate, methyl crotonate, and methyl butanoate. H-abstraction reactions are treated in line with the systematic approach described

Table 1
High temperature decomposition and oxidation reactions of methyl esters.

	Reaction[a]	A	n	E_a	Ref
Methyl formate					
R1	MF ⇆ $CH_3OH + CO$	2.0×10^{13}	0	60,000	[42]
R2	MF ⇆ $CH_4 + CO_2$	1.5×10^{12}	0	59,800	[42]
R3	MF ⇆ $2\ CH_2O$	1.0×10^{12}	0	61,000	[42]
R4	MF → $CH_3 + CO_2 + H$	2.2×10^{24}	−2.4	97,600	This work
R5	$CH_3OCO + H$ ⇆ MF	1.0×10^{11}	0	0	[42]
R6	$CH_3O + HCO$ ⇆ MF	3.0×10^{10}	0	0	[42]
R7	$H + MF \rightarrow H_2 + CH_2O + HCO$	1.6×10^{11}	0	10,500	This work
R8	$H + MF \rightarrow H_2 + CH_3OCO$	5.3×10^{10}	0	10,500	This work
R9	$R + MF \rightarrow RH + CH_2O + HCO$	$3H^{Ester}_{Prim}$			See text
R10	$R + MF \rightarrow RH + CH_3OCO$	$1H^{Ester}_{Prim}$			See text
R11	CH_3OCO ⇆ $CO_2 + CH_3$	1.55×10^{12}	0.514	15,200	[54]
R12	CH_3OCO ⇆ $CO + CH_3O$	7.4×10^{12}	0.479	23,800	[54]
Methyl acrylate and methyl crotonate					
R13	$MA \rightarrow C_2H_3 + CH_3 + CO_2$	2.0×10^{16}	0	85,000	This work
R14	$OH + MA$ ⇆ $CH_3CHO + CH_3OCO$	2.0×10^{9}	0	0	This work
R15	$OH + MA \rightarrow C_2H_4 + CO_2 + CH_3O$	1.0×10^{9}	0	0	This work
R16	$OH + MA \rightarrow CH_2O + CH_2CO + CH_3O$	1.0×10^{9}	0	0	This work
R17	$H + MA$ ⇆ $C_2H_3CHO + CH_3O$	2.0×10^{10}	0	3000	This work
R18	$H + MA$ ⇆ $C_2H_4 + CH_3OCO$	2.0×10^{10}	0	3000	This work
R19	$R + MA \rightarrow RH + CH_2O + CO + C_2H_3$	$3H^{Ester}_{Prim}$			See text
R20	$R + MA \rightarrow RH + C_2H_2 + CH_3OCO$	$3H_{Vinyl}$			See text
R21	$MC \rightarrow CHCHCH_3 + CO_2 + CH_3$	5.0×10^{16}	0	82,000	[35]
R22	$MC \rightarrow CHCHCH_3 + CH_3OCO$	3.5×10^{15}	0	84,439	This work
R23	$MC \rightarrow pC_3H_4 + MF$	1.0×10^{14}	0	68,000	This work
R24	$H + CH_2{=}CH\text{-}\bullet CH\text{-}C(O)\text{-}O\text{-}CH_3$ ⇆ MC	2.0×10^{11}	0	0	
R25	$CH_2{=}CH\text{-}\bullet CH\text{-}C(O)\text{-}O\text{-}CH_3 \rightarrow CH_3O + C_2H_2 + CH_2CO$	1.0×10^{13}	0	49,000	This work
R26	$OH + MC \rightarrow CH_3CHO + CH_2CO + CH_3O$	1.0×10^{9}	0	0	This work
R27	$H + MC$ ⇆ $MA + CH_3$	1.2×10^{10}	0	2000	This work
R28	$H + MC \rightarrow C_2H_4 + CH_2CO + CH_3O$	1.0×10^{10}	0	2000	This work
R29	$H + MC$ ⇆ $C_3H_6 + CH_3OCO$	1.0×10^{10}	0	2000	This work
R30	$R + MC \rightarrow RH + CH_2{=}CH\text{-}\bullet CH\text{-}C(O)\text{-}O\text{-}CH_3$	$2H^{\alpha}_{Sec}$			See text
R31	$R + MC \rightarrow RH + CHCHCH_3 + CO + CH_2O$	$3H_{Prim}$			See text
R32	$R + MC \rightarrow RH + 0.5\ aC_3H_4 + 0.5\ pC_3H_4 + CH_3OCO$	$1H_{Vinyl}$			See text
Methyl butanoate					
R33	$MB \rightarrow CO_2 + nC_3H_7 + CH_3$	5.0×10^{16}	0	86,800	This work
R34	$MB \rightarrow CH_2CO + CH_3O + C_2H_5$	5.0×10^{16}	0	85,200	This work
R35	MB ⇆ $CH_3OCO + nC_3H_7$	5.0×10^{16}	0	89,900	This work
R36	MB ⇆ $\bullet CH_2\text{-}CH_2\text{-}C(O)\text{-}O\text{-}CH_3 + CH_3$	5.0×10^{16}	0	88,900	This work
R37	$C_2H_4 + CH_3OCO$ ⇆ $\bullet CH_2\text{-}CH_2\text{-}C(O)\text{-}O\text{-}CH_3$	2.1×10^{8}	0	7350	[42]
R38	$H + RMBX$ ⇆ MB	1.0×10^{11}	0	0	[35]
R39	$H + MB \rightarrow MF + nC_3H_7$	1.0×10^{10}	0	4000	This work
R40	$H + MB \rightarrow H_2 + RMBX$	1.0×10^{12}	0	7925	This work
R41	$R + MB \rightarrow RH + RMBX$	$6H_{Sec}$			See text
R42	$O_2 + RMBX$ ⇆ $HO_2 + MC$	2.5×10^{9}	0	6000	[27]
R43	$RMBX \rightarrow H + MC$	1.0×10^{14}	0	42,000	This work
R44	RMBX ⇆ $MA + CH_3$	7.0×10^{12}	0	29,000	This work
R45	$RMBX \rightarrow C_2H_4 + CH_3O + CH_2CO$	1.1×10^{14}	0	33,000	This work
R46	$RMBX \rightarrow C_3H_6 + CH_3 + CO_2$	3.5×10^{13}	0	33,000	This work

MF = methyl formate.
MA = methyl acrylate.
MC = methyl crotonate.
MB = methyl butanoate.
RMBX = lumped radical of methyl butanoate.
[a] $k = A\ T^n \exp(-E_a/RT)$. Units are: mole, l, s, K and cal.

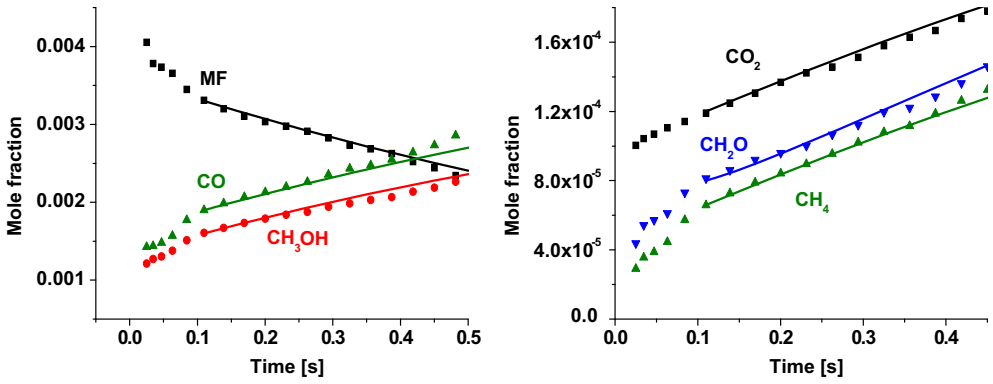

Fig. 2. Methyl formate pyrolysis in the Princeton flow reactor [41] (0.5% MF in N_2 at 3 atm and 975 K).

elsewhere [51]. According to the bond dissociation energies of the H atoms, the rate of H-abstraction from different sites are simply obtained by using the reference kinetic parameters of the removal of primary H atoms (H_{prim}) and the specific correction factor of the *H* atoms to be removed. Thus, the primary *H* atoms in the methyl of ester group ($3H^{Ester}_{Prim}$) are assumed to be 1.5 times more reactive than the primary *H* atoms in alkanes. Similarly, the rate parameters to abstract the secondary *H* atoms ($2H^{\alpha}_{Sec}$) in the α position to the ester group to form the radical CH_2 = CH-•CH-C(O)-O-CH_3 are assumed twice as reactive as the usual secondary *H* atoms in alkanes.

Low temperature oxidation reactions are not included as they would be expected to play a very limited role and because of the lack of relevant experimental data in this region. The whole kinetic scheme POLIMI_TOT1112 is available at the website: http://creckmodeling.chem.polimi.it/.

A first simple and useful validation test refers to the pyrolysis of 0.5% mol of methyl formate in N_2 at 975 K, in the pressurized flow reactor of Princeton at 3 atm. Following the suggestions of Dooley et al. [42] and Zhao et al. [52], the experiments are conveniently modeled as an isobaric and adiabatic plug flow reactor only after the inlet/mixing initial zone. Fig. 2 shows the comparison of model predictions and experiments. All over the text, symbols correspond to experimental results and lines to simulations. The role of molecular reactions is evident. More than 80% of the MF decomposes, forming methanol via the molecular path, while direct formation of CH_4 and CH_2O is significantly lower. The significant role of the molecular reactions is due to the high activation energies of the chain initiation reactions of methyl formate R4 and the reverse of R5 and R6. Of course, these reactions and the radical paths become more significant in flame conditions. The limited radical decomposition follows a radical path with a prevailing formation of •CH_2OCHO, here considered as instantaneously transformed into CH_2O and HCO. We, on the contrary, maintain the two decomposition channels of the methoxy-carbonyl radical (CH_3OCO•) to form either CO_2 + CH_3• or CO + CH_3O•. According to Farooq et al. [53], model predictions based on the original Fisher et al. mechanism [14] underestimate the CO_2 yields during pyrolysis, thus we improved CO_2 predictions by using the rates of the CH_3OCO• channels of the methyl butanoate model of Huynh and Violi [54,55]. In fact, the selectivity of the CO_2 channel is more than 90% in these conditions, while similar CO and CO_2 selectivities were predicted by using the previous kinetics [14].

A second validation test is provided by the ignition delay times of MF oxidation in Ar in the Galway shock tube device in the temperature range 1300–1900 K, at varying pressures from 2.7 up to 9.2 atm. Fig. 3 shows model comparisons with the experiments at equivalent ratios $\Phi = 0.5, 1$ and 2. As already observed by Dooley et al. [41], MF is essentially reacting as a mixture of methanol and carbon monoxide doped with methane, carbon dioxide, and formaldehyde.

Model predictions agree satisfactorily with the ignition delay times, even if the reactivity and the apparent activation energy are slightly over-predicted, mainly in lean conditions.

Dooley et al. [42] studied the oxidation of methyl formate in a series of burner stabilized laminar premixed flames at low pressures and different equivalence ratios in argon. Fig. 4 shows a further comparison of model predictions and experiments at flame conditions of 25.2% fuel, Φ = 1.0 at 22 Torr. Panel a) of the

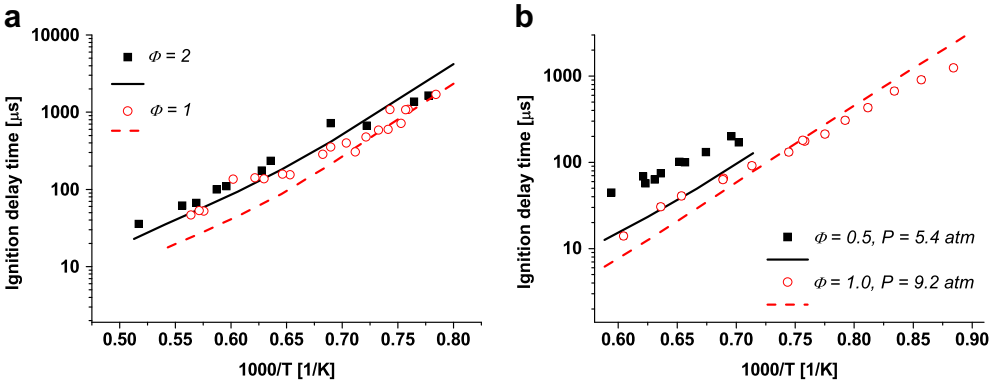

Fig. 3. Methyl formate ignition delay times in a shock tube [41]. Panel a) 2.7 atm: MF/O_2/Ar, 0.5/0.5/99.0, Φ = 2.0, and MF/O_2/Ar, 0.5/1.0/98.5, Φ = 1.0. Panel b) 5.4 atm: MF/O_2/Ar, 0.5/2.0/97.5, Φ = 0.5, and 9.2 atm: MF/O_2/Ar, 2.5/5.0/92.5, Φ = 1.0.

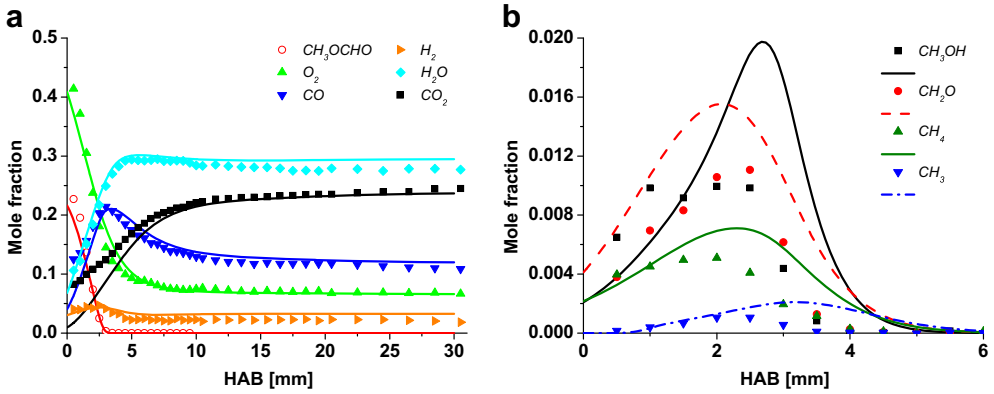

Fig. 4. Low pressure laminar premixed flame of methyl formate. Dooley et al. [42]. Panel a) Flame structure. Panel b) Comparison of major intermediate products.

figure shows major species mole fraction as a function of the height above the burner (HAB). The temperature profile experimentally determined by Dooley et al. [42] was used in these calculations. Flame structure is properly predicted. Panel b) of the same figure shows major intermediates mole fraction profiles. Methanol and formaldehyde are the main products detected and significant amounts of CH_4 and CH_3 are also present. The model reasonably predicted peaks and trends of these species. However, an overall over-prediction is observed. Flux analysis on methyl formate indicates that most of the fuel (67%) is consumed by molecular reactions, mainly to form CH_3OH and CO. The remaining fuel consumption is mainly attributed to propagation reactions to form primary radicals (32%), while initiation reactions account for ~1%. Propagation reactions and subsequent β-decomposition reactions promote CO_2 and methyl radical formation as well as CH_2O and HCO radical. Propagation reactions mainly occur at early stage of the flame (*i.e.* lower temperatures) with respect to molecular reactions. For these reasons, CH_2O and CH_4 formation happens earlier than CH_3OH formation. As observed by Dooley et al. [42], the small quantities of C_2H_4 (mole fraction in the order of 10^{-3}) are explained via methyl radical recombination with $\bullet CH_2OCHO$ to form ethyl formate. Successive H-abstraction and four center molecular reaction of ethyl formate form C_2H_4. Still considering the lumped model and in order to restrain the total

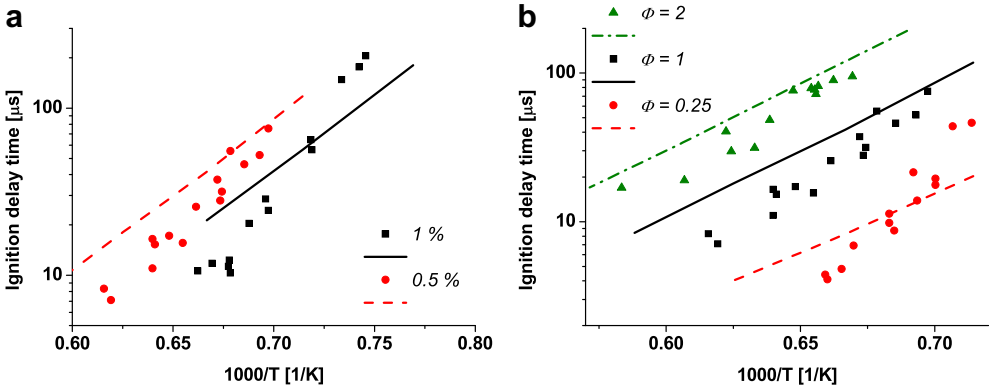

Fig. 5. Methyl acrylate ignition delay times in shock tube experiments at 7.5–9 atm [28]. Panel a) Effect of fuel mole fraction at $\Phi = 1$. Panel b) Effect of Φ at fuel mole fraction 0.5%.

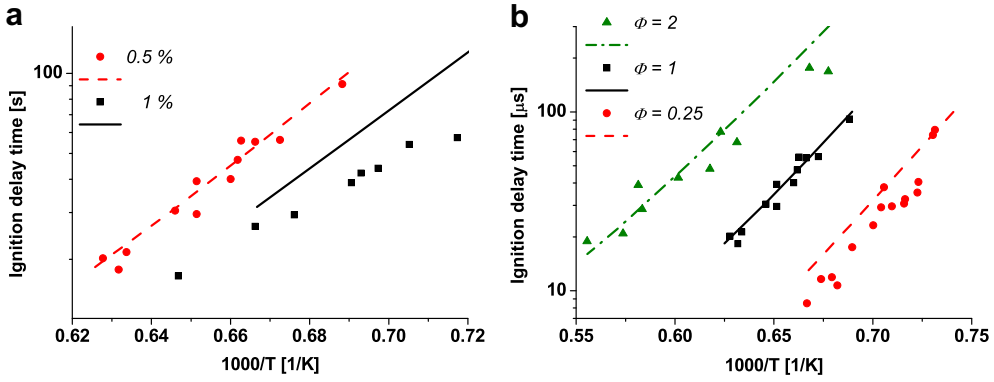

Fig. 6. Methyl crotonate ignition delay times in shock tube experiments at 7.5–9 atm [28]. Panel a) Effect of fuel mole fraction at $\Phi = 1$. Panel b) Effect of Φ at fuel mole fraction 0.5%.

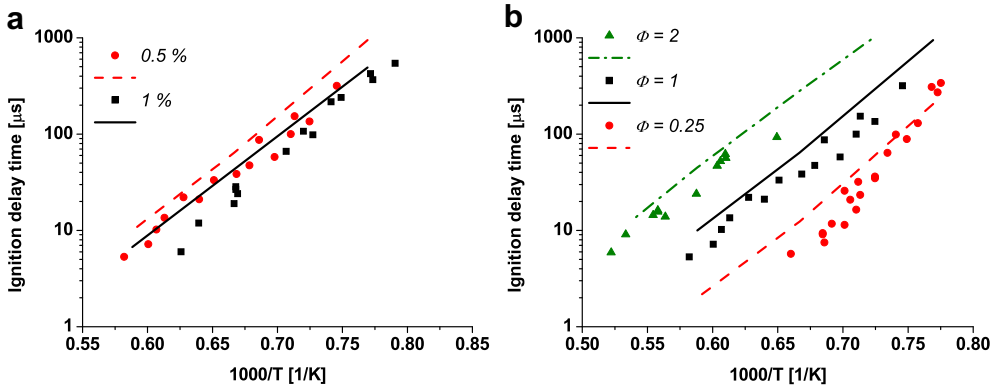

Fig. 7. Methyl butanoate ignition delay times in shock tube experiments in argon at 8.5 atm [27]. Panel a) MB concentration 0.5% and 1%, at $\Phi = 1$. Panel b) $\Phi = 0.25$, 1, and 2, at MB concentration 0.5%.

number of species involved in the kinetic scheme, we do not include $\bullet CH_2OCHO$ radical and ethyl formate in the present kinetic model.

4. Methyl acrylate and methyl crotonate

Methyl acrylate (MA) and methyl crotonate (MC) are significantly present during the decomposition and oxidation of large methyl esters. Thus, the interest in their kinetics is due not only for the simple chemical structure but also for the effective role during the successive reaction steps of larger biofuels. Detailed mechanisms for the combustion of the methyl acrylate and methyl crotonate, together with the corresponding ethyl esters, automatically generated using EXGAS software, have been presented and discussed by Bennadij et al. [28]. The model was validated in comparison with the ignition delay times measured behind reflected shock waves in a wide temperature range from 1280 to 1930 K, at pressures of 7–9.65 atm, and different equivalence ratios. The relative importance of the main reaction pathways, derived from flow rate and sensitivity analyses, are discussed herein.

Table 1 reports the small subset of decomposition and oxidation reactions useful to extending the simulation capabilities of the overall kinetic model to these two methyl esters. Note that methyl crotonate is considered here as a lumped species describing both the methyl-2-butenoate and methyl-3-butenoate. While the first isomer is a relevant intermediate of methyl butanoate decomposition, the second is the prevailing one when the decomposition of large methyl esters is considered. The consistency of this lumping seems viable because both these isomers easily produce the same resonantly stabilized radicals:

$$\begin{aligned} CH_2 &= CH - {}^{\bullet}CH - C(O) - O - CH_3 \leftrightarrow {}^{\bullet}CH_2 - CH \\ &= CH - C(O) - O - CH_3 \end{aligned}$$

Figs. 5 and 6 compare the model predictions with the ignition delay times measured in the shock tube experiments of MA and MC, reported by Bennadij et al. [28].

Addition reactions of H and OH radicals on the double C-C bond of the unsaturated methyl esters, typically MA and MC, significantly compete with the H-abstraction reactions. Ethylene and acrolein are the products of H additions on methyl acrylate, while acetaldehyde is formed from OH additions:

$$\begin{aligned} H + CH_2 &= CH - C(O) - O - CH_3 \leftrightarrow [{}^{\bullet}CH_2 - CH_2 - C(O) - O - CH_3] \\ &\leftrightarrow C_2H_4 + {}^{\bullet}C(O) - O - CH_3 \end{aligned} \quad (R18)$$

$$\begin{aligned} OH + CH_2 &= CH - C(O) - O - CH_3 \leftrightarrow [{}^{\bullet}CH_2 - C(OH)H - C(O) \\ &- O - CH_3] \leftrightarrow CH_3CHO + {}^{\bullet}C(O) - O - CH_3 \end{aligned} \quad (R14)$$

Propylene and methyl acrylate are the main intermediates from H additions on the double C-C bond of methyl crotonate, while ketene and acetaldehyde are formed from OH additions. Thus, more reactive species are formed from MA, thereby justifying the shorter ignition delay times of methyl acrylate compared to methyl crotonate. The ignition delay times of MA are generally over-predicted. The large deviations in the activation energy of these delay times at lean conditions ($\Phi = 0.25$) could suggest that either the kinetics

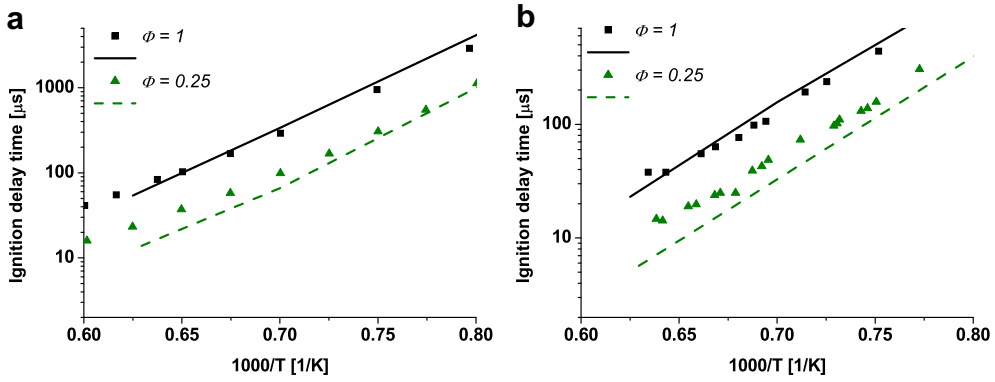

Fig. 8. Methyl butanoate ignition delay times in shock tube experiments [16]. Panel a) 1.0% MB at 1 atm and $\Phi = 1.0$ and 0.25. Panel b) 1.0% MB at 4 atm and $\Phi = 1.0$ and 0.25.

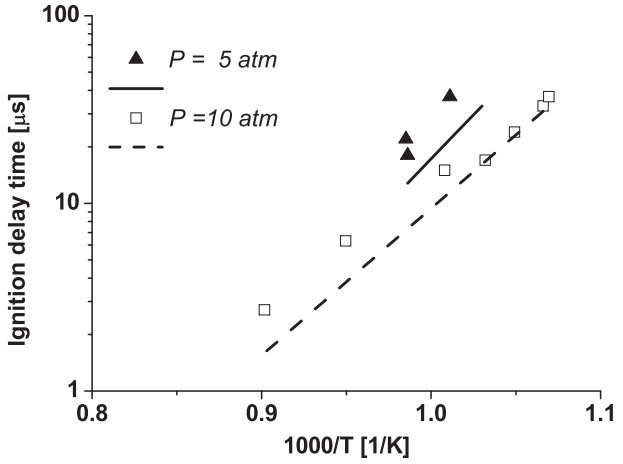

Fig. 9. Rapid compression machine experiments. Methyl butanoate (~1.27%) in N_2/Ar mixtures at $\Phi = 0.4$ [20].

need to be improved or the experiments need to be critically verified or extended.

5. Methyl butanoate

5.1. Shock tube experiments

Hakka et al. [27] studied the ignition delay times of MB (0.5 and 1%) oxidation in argon mixtures behind the reflected shock wave at high temperatures (1280–1990 K) and pressures of 7.6–9.1 atm, at three different equivalence ratios ($\phi = 0.25$, 1, and 2). Fig. 7 reports comparisons between model predictions and experiments. Model predictions properly capture both the shorter delay times at higher fuel concentration (Panel a) and the clear increase in the reactivity in leaner conditions (Panel b). Model results systematically underestimate the reactivity of the system, *i.e.* model over-predicts ignition delay times.

Higher reactivity of the model is, on the contrary, generally observed in comparison with both Dooley et al. [16] and Walton et al. [20] experiments, discussed below. Dooley et al. [16] studied the ignition delay times of high temperature MB oxidation at a reflected shock pressure of 1 and 4 atm and different equivalent ratios. Fig. 8a and b show comparisons between model predictions and experimental measurements. While predicted delay times agree with experiments at stoichiometric conditions, the model slightly underpredicts the ignition delay times in lean conditions. Walton et al. [20] studied the MB ignition using a rapid compression machine at temperatures between 935 and 1117 K. Fig. 9 compares predicted and experimental ignition delay times at ~5 atm and ~10 atm and $\Phi = 0.4$. Again the model slightly over-predicts MB reactivity in these conditions.

5.2. Pressurized flow reactor

Marchese et al. [40] presented experiments of MB oxidation in the Princeton pressurized flow reactor at 12.5 atm, at different equivalent ratios. 800 ppm of fuel are oxidized at different temperatures between 600 and 900 K, and at a residence time of 1.8 s Fig. 10 shows the comparisons between experiments and simulations of the mole fraction of major species from MB oxidation at 12.5 atm and 1.8 s vs the reactor temperature. CO and CO_2 selectivities are properly predicted, while CH_2O is over-predicted. The experimental measurements show that the ignition of the mixture takes place from ~800 and 850 K, depending on the equivalent ratio. Model results are accurate for the

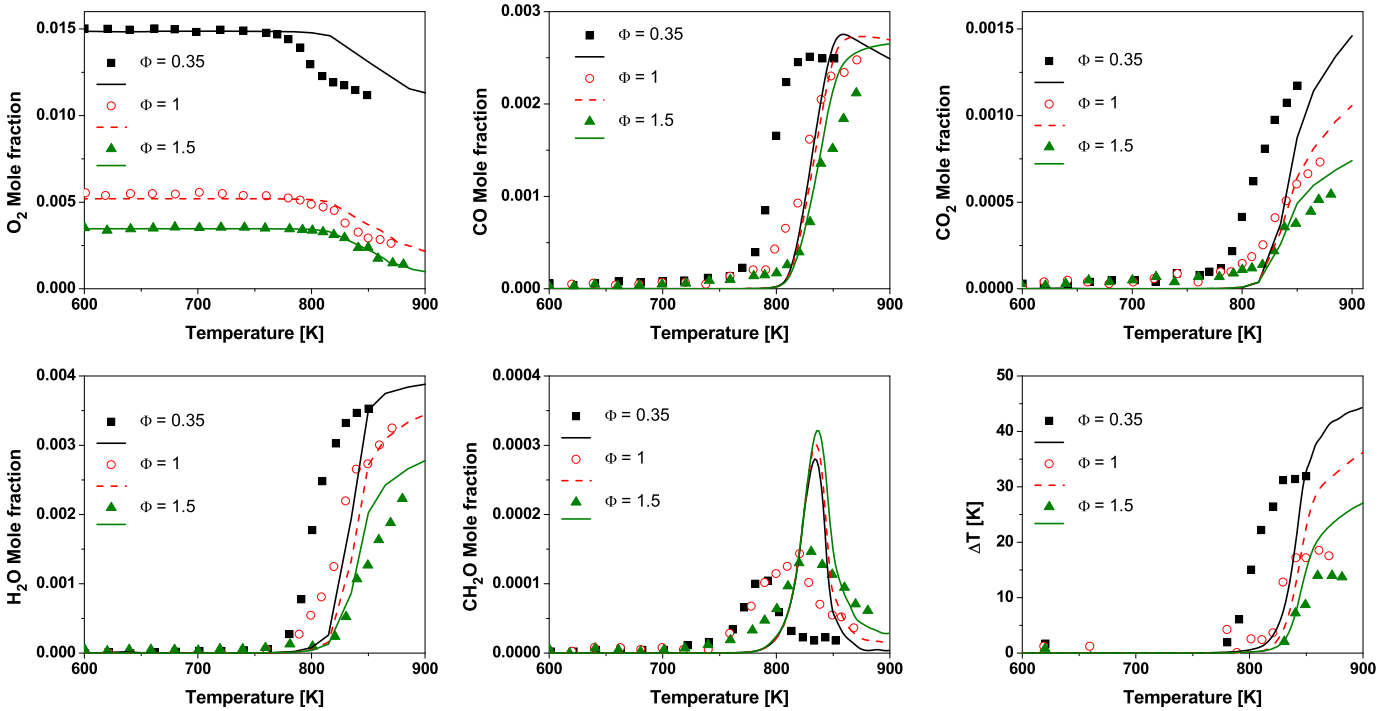

Fig. 10. Flow reactor data at different temperatures. Major species from the oxidation of 800 ppm methyl butanoate at 12.5 atm, residence time of 1.8 s, and $\Phi = 0.35$, 1.0 and 1.5 [40].

stoichiometric and fuel rich mixtures. The model underpredicts the reactivity of the lean mixture and there is a deviation of ~30 K.

5.3. Oxidation of methyl butanoate in a JSR

The oxidation of methyl butanoate was carried out in the quartz jet stirred reactor at Nancy at a constant temperature and pressure [27]. Due to undesired reactions between MB and seals inside the flow meters, only a couple of experimental conditions were tested. The oxidation of 2% of MB was studied at 800 K for an equivalence ratio of 0.5 and at 850 K for an equivalence ratio of 1. Fig. 11 shows the time evolution profiles of major species during MB oxidation in these operating conditions. Model predictions well agree with experimental measurements at 800 K, but an over-prediction of MC is observed. At 850 K, the model correctly predicts MA and MB but over-predicts MB conversion and CO_2 yields, with a significant under estimation of ethylene. Similar deviations were also observed with the detailed mechanism of Hakka et al. [27].

5.4. Methyl crotonate and methyl butanoate oxidation in a JSR

Gaïl et al. [35,36] and Sarathy et al. [37] studied and compared the decomposition and oxidation behavior of methyl crotonate and methyl butanoate. Namely, MC and MB oxidation was compared in an atmospheric JSR under N_2 dilute conditions over the temperature range 850–1400 K, at different equivalence ratios and a residence time of 0.07 s Figs. 12 and 13 compare experiments and model predictions of several species from the two fuels at different equivalent ratios ($\Phi = 0.75$ and 1.13).

The comparison between predicted and experimental conversion of both the fuels clearly indicates an under estimation of predicted reactivity at temperatures lower than 1000–1100 K, both in lean and rich conditions. A similar deviation is also present and

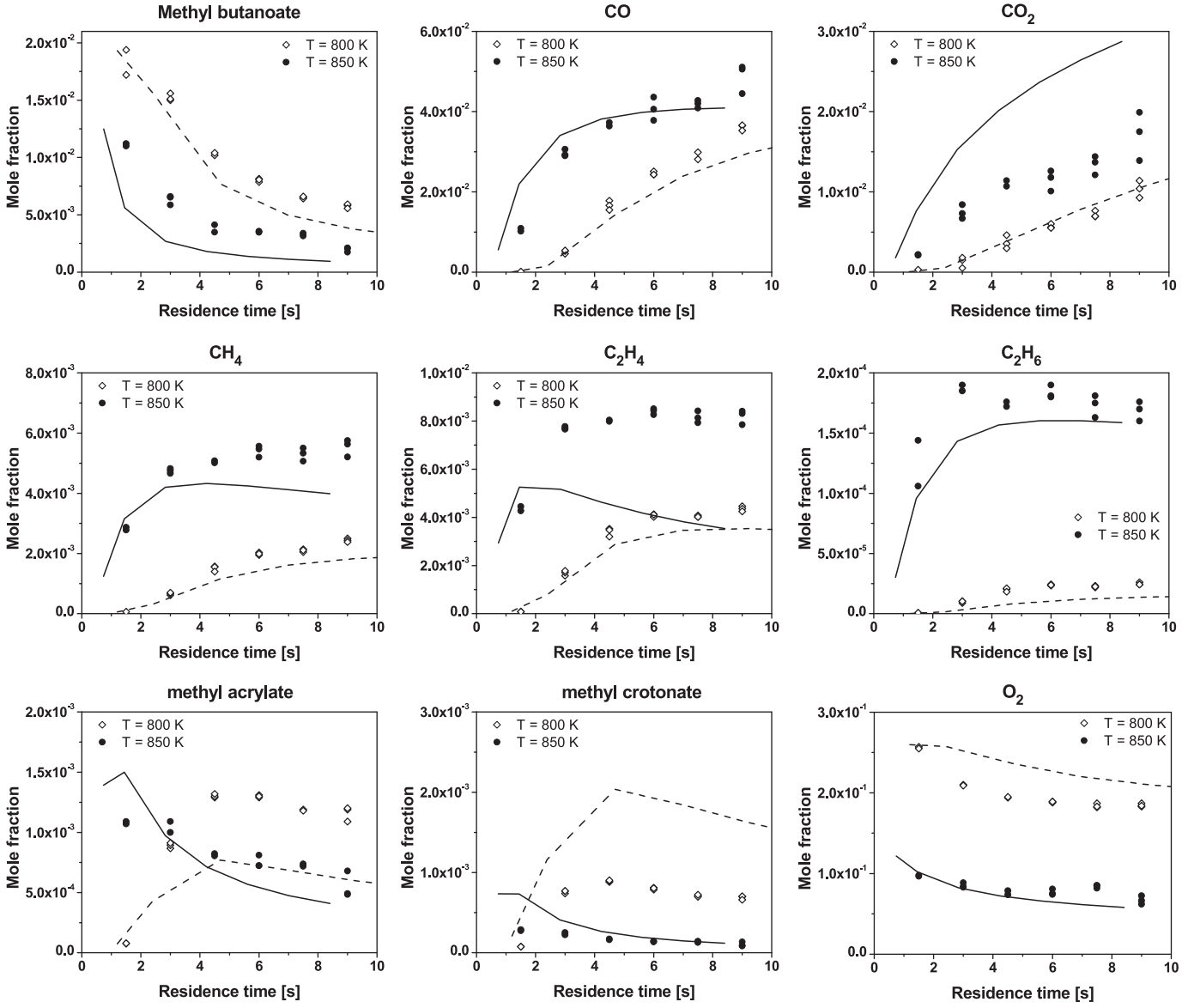

Fig. 11. Time evolution profiles of major species during the oxidation of methyl butanoate in an atmospheric JSR at 800 K and $\Phi = 0.5$, and at 850 K and $\Phi = 1$ [27].

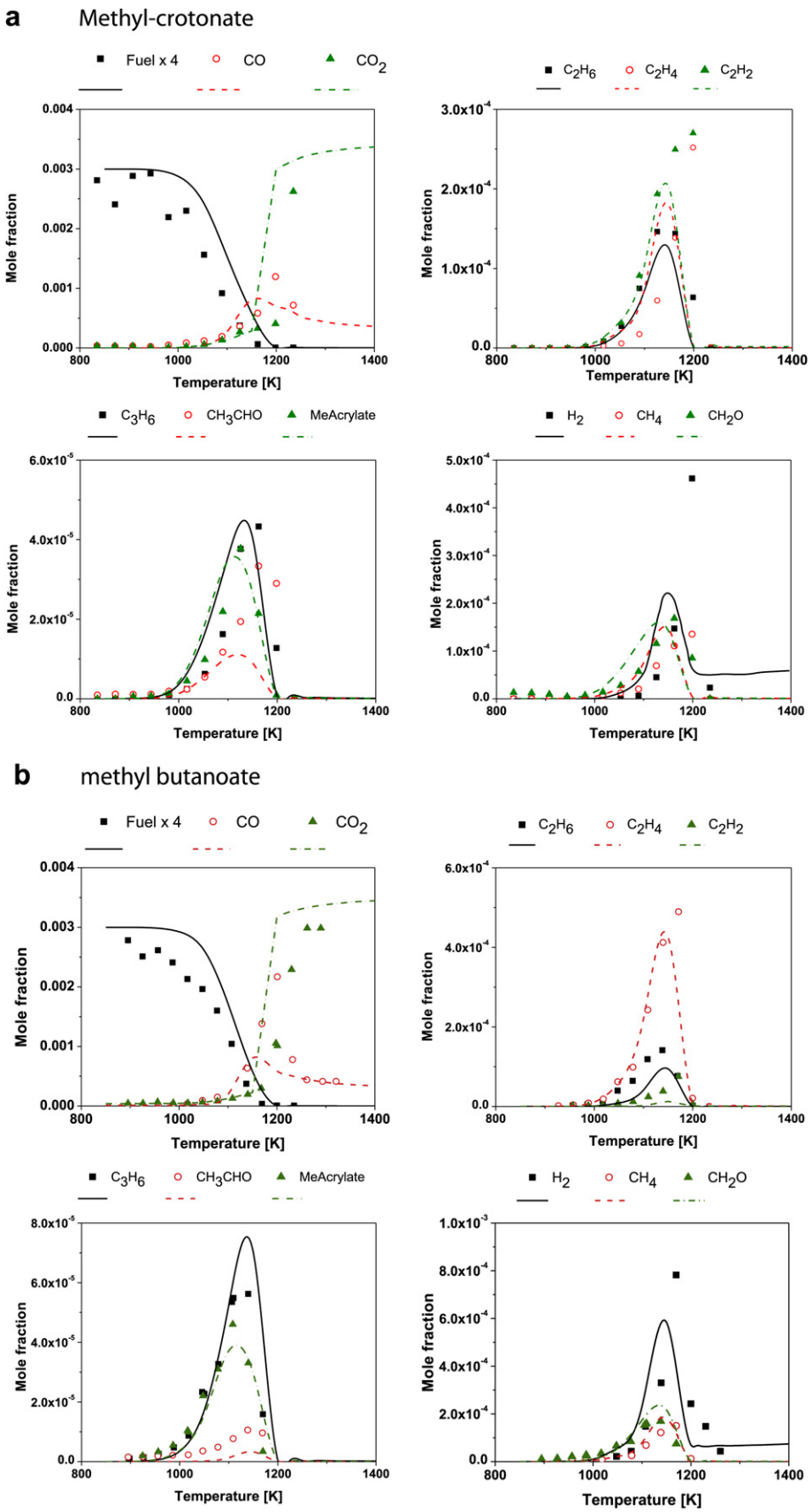

Fig. 12. Experimental results and model predictions of major products from methyl crotonate (panel a) and methyl butanoate (panel b) oxidation in the JSR at $\Phi = 0.75$, atmospheric pressure and 0.07 s [36].

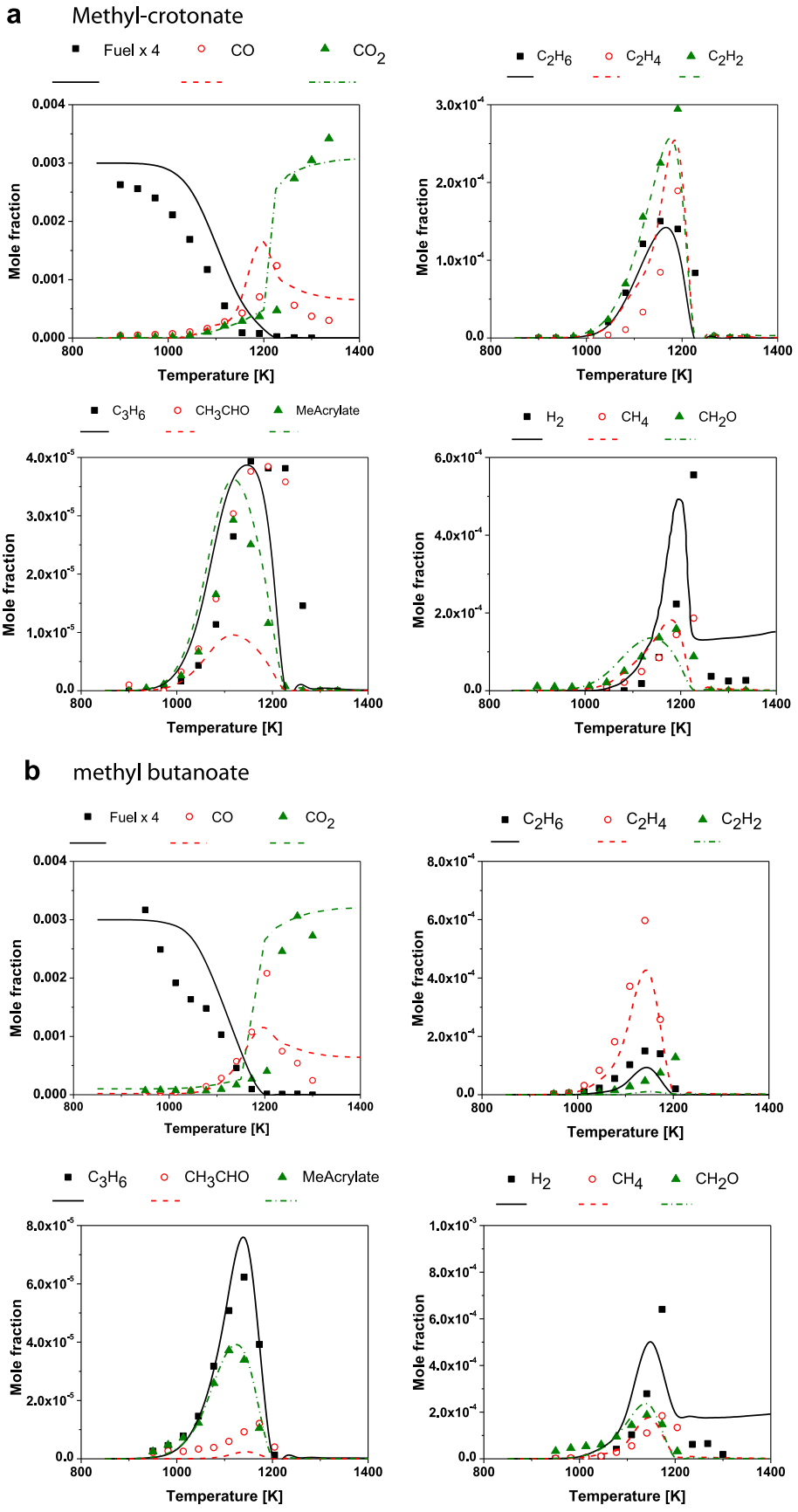

Fig. 13. Experimental results and model predictions of major products from methyl crotonate (panel a) and methyl butanoate (panel b) oxidation in the JSR at $\Phi = 1.13$, atmospheric pressure and 0.07 s [36].

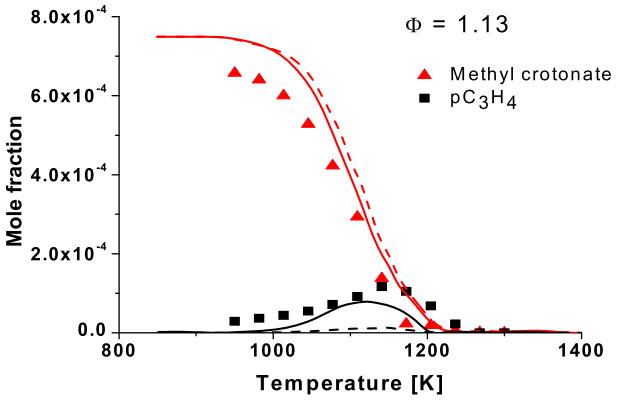

Fig. 14. Methyl crotonate oxidation in JSR [36]. Comparison of methyl crotonate conversion and propyne formation with (solid lines) and without (dashed lines) reaction 23 of Table 1.

observed when using the detailed kinetic model of Gail et al. [26] for MB and MC oxidation.

Experimental data mainly show relevant early MC reactivity where there is a significant amount of methyl-acetylene (pC_3H_4) and methanol. It is quite difficult to explain pC_3H_4 formation via H-abstraction on the vinylic site and/or via dehydrogenation of vinyl radicals of MC. It is likely that this reactivity is the result of catalytic activity of the reactor surfaces with the net result of a significant conversion of MC (and MB). One way to reduce these systematic deviations between model predictions and experiments is to introduce the following molecular reaction:

$$CH_3CH=CH-C(O)-O-CH_3 \leftrightarrow CH_3C\equiv CH+H-C(O)-O-CH_3$$
$$k=1\times10^{14}\exp(-68{,}000/RT)\left[s^{-1}\right]$$

Fig. 14 shows a comparison of model predictions with and without this apparent reaction. Decomposition of MC and MB follow very different reaction paths. This discussion is analyzed in-depth in the papers previously referred to. Therefore we limit our discussion to a few relevant features and to the major reaction paths reported in Fig. 15. MC decomposition, apart from the aforementioned reaction R23, is ruled by the unimolecular radical chain initiation reaction R21 to form methyl radical from the methoxy group. H addition reactions to form MA (R27), ethylene (R28), and propylene (R29) are of the same importance as the H-abstraction reactions (R30)–(R32), dominated by H, OH and CH_3 radicals. The radical in the α-position ($CH_2=CH\text{-}\bullet CH\text{-}C(O)\text{-}O\text{-}CH_3$) is the prevailing H-abstraction product from MC and is a relevant source of vinyl-ketene. This component is not considered in the lumped kinetic scheme and the following direct decomposition reaction is assumed:

$$CH_2=CH-\bullet CH-C(O)-O-CH_3 \leftrightarrow [CH_2=CH-CH=C(O)+\bullet O-CH_3] \leftrightarrow CH\equiv CH+CH_2=CO+\bullet O-CH_3 \quad (R25)$$

This is a source of acetylene, together with the demethylation of the $CHCHCH_3$ radical formed in the initiation reaction R21.

The role of H-abstraction reactions (R41) is dominant for MB decomposition. In this case, H is the most important abstracting radical, while OH and CH_3 play a minor role. Ethylene, MA and propylene are the major primary products from the decomposition of the lumped MB radical (R44 − R46).

Figs. 12 and 13 clearly show the significant initial formation of acetylene, while ethylene is a secondary product for MC oxidation. Ethane is formed via the methyl radical recombination reaction, both from MB and MC decomposition. The model agrees fairly well with the experimental data, showing the increase in C2 species in rich conditions, even though it systematically underpredicts the maximum yields at high temperatures. C2 species clearly indicate a completely different behavior for MB. Ethylene is the primary most abundant product, while acetylene is only a secondary product. MA and propylene are primary products from both fuels and are formed in larger amounts from MB.

6. Laminar flame speeds

Panel a) of Fig. 16 reports a comparison of the premixed laminar flame speeds of MF with the experimental measurements of Dooley et al. [41]. Due to the importance of methanol chemistry in MF combustion, the laminar flame speeds of methanol are also reported and compared with experimental data in the same figure [56]. Panel b) compares the predicted laminar flame speeds of methyl crotonate with the experiments of Wang et al. [57].

Panel c) compares the experimental measurements and the predicted laminar flame speeds of methyl butanoate and n-butane in air at 403 K and 1 atm [57]. It is evident from this figure that flame speeds of MB are slightly lower than the ones of the corresponding n-alkane. This fact is mainly due to the slightly lower adiabatic flame temperatures of methyl esters in respect of n-alkanes. Finally, Panel d) shows the pressure effect (1 and 2 atm) on the laminar flame speeds of methyl butanoate/air

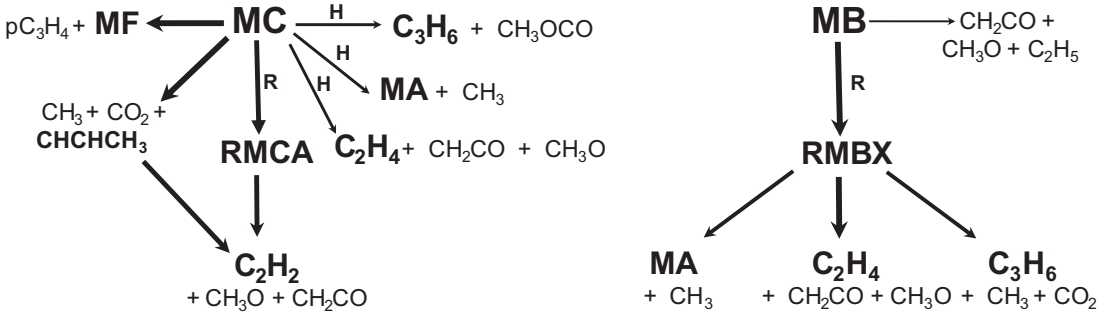

Fig. 15. Major reaction paths of methyl crotonate and methyl butanoate oxidation in JSR with the conditions of Fig. 13 at ~50% fuel decomposition. The thickness of the arrows represents the relative importance of the reaction path.

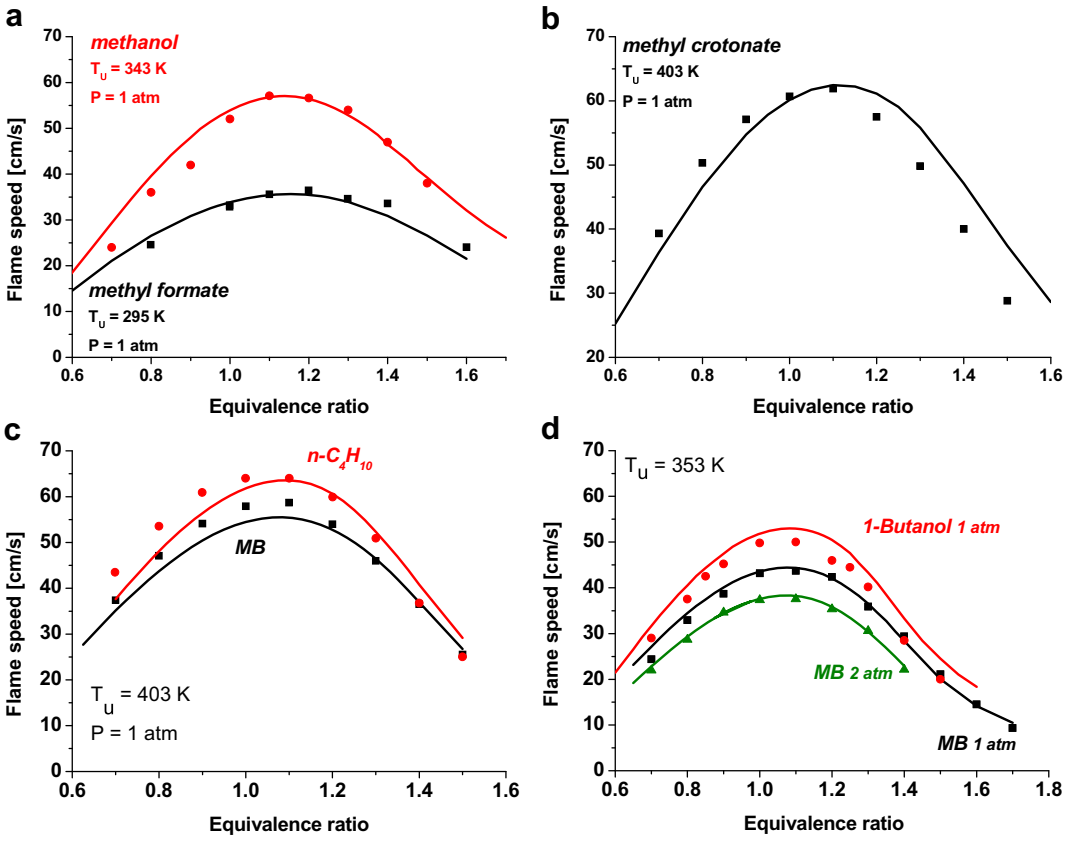

Fig. 16. Premixed laminar flame speeds in air. Panel a) Methyl formate at 295 K and 1 atm [41]; Methanol at 343 K and 1 atm [56]. Panel b) Methyl crotonate at 403 K and 1 atm [57]. Panel c) Methyl butanoate and n-butane at 403 K and 1 atm [57]. Panel d) Methyl butanoate at 353 K (1 and 2 atm) and 1-butanol at 353 K and 1 atm [58].

mixtures at 353 K [58]. As a matter of further comparison, the same figure also shows the laminar flame speeds of 1-butanol at 1 atm. Model predictions agree well with the data of Liu [58], while a slight under-prediction is observed compared to the data of Wang [57]. According to the lower adiabatic flame temperature, the predicted flame speed of methyl butanoate is lower than those of both n-butane and 1-butanol, as experimentally established [57,58].

Fig. 16 demonstrates the reliability of the kinetic model in properly characterizing laminar flame speeds of small methyl esters. On these bases, panel a) of Fig. 17 directly compares the predicted laminar flame speeds of the small methyl esters in air, at the same flame conditions (T_0 = 403 K and 1 atm). Panel b of the same figure shows the corresponding maximum flame temperatures, while panel c) and d) report the peak concentration of H, CH_3, OH and C_2H_3 radicals. This analysis and comparison highlight several interesting features.

Firstly, the flame speeds of unsaturated esters are higher than the one of methyl butanoate. The lowest speed of MB is explained quite well on the basis of the lower adiabatic flame temperature. This behavior is the same as already observed for alkanes and alkenes.

With similar flame temperatures, methyl acrylate flame speed is higher than that of methyl crotonate. Again there is a clear similarity to the behavior of ethylene and propylene flames where the difference in flame speed is due both to larger formation of vinyl radical in the ethylene flame and to the larger formation of the resonantly stabilized allyl (C_3H_5) radical in the propylene flame. MA flame shows a C_2H_3 radical peak concentration about double that of the MC (and MB) flame. Sensitivity analysis on MA flame speed at $\Phi = 1$, reported in Fig. 18, confirms the importance of the branching reaction:

$$C_2H_3 + O_2 \leftrightarrow CH_2CHO + O$$

thus explaining the highest reactivity of MA, in these conditions. Moreover, the MC flame shows the highest methyl radical concentration whose inhibiting effect on flame speed is well established [59] as well as a lower H radical concentration (see panel c) of Fig. 17). Sensitivity analysis on the flame speed of MA and MC further highlights that the most sensitive reactions belong to the H_2/CO system. Fuel-specific reactions of methyl crotonate show the negative effect of the H addition reaction R29 due to the formation of propylene, precursor of the resonant allyl radical. Similarly, the H radical scavenging effect of reaction R18 reduces the flame speed of MA, while the H addition R17, with acrolein formation, has a positive sensitivity coefficient in rich conditions.

Furthermore, the flame speed of methyl formate exhibits a different shape with a maximum at $\Phi = \sim 1.2$, while the remaining esters peak at ~1.1. Flame speeds of MF in rich conditions approach those of methyl acrylate, despite the lower flame temperatures. Peak concentrations of H and CH_3 radicals (panel c) confirm this behavior. As already discussed, methyl formate either forms methanol, via the molecular path, or mostly decomposes to form formaldehyde. For this reason peak concentrations of CH_3 radical are lowest in the MF flame. On the contrary, peak concentrations of hydrogen radical, mainly formed via HCO decomposition, are highest in rich conditions. Both the high H and the low CH_3 concentrations promote system reactivity and higher flame speed.

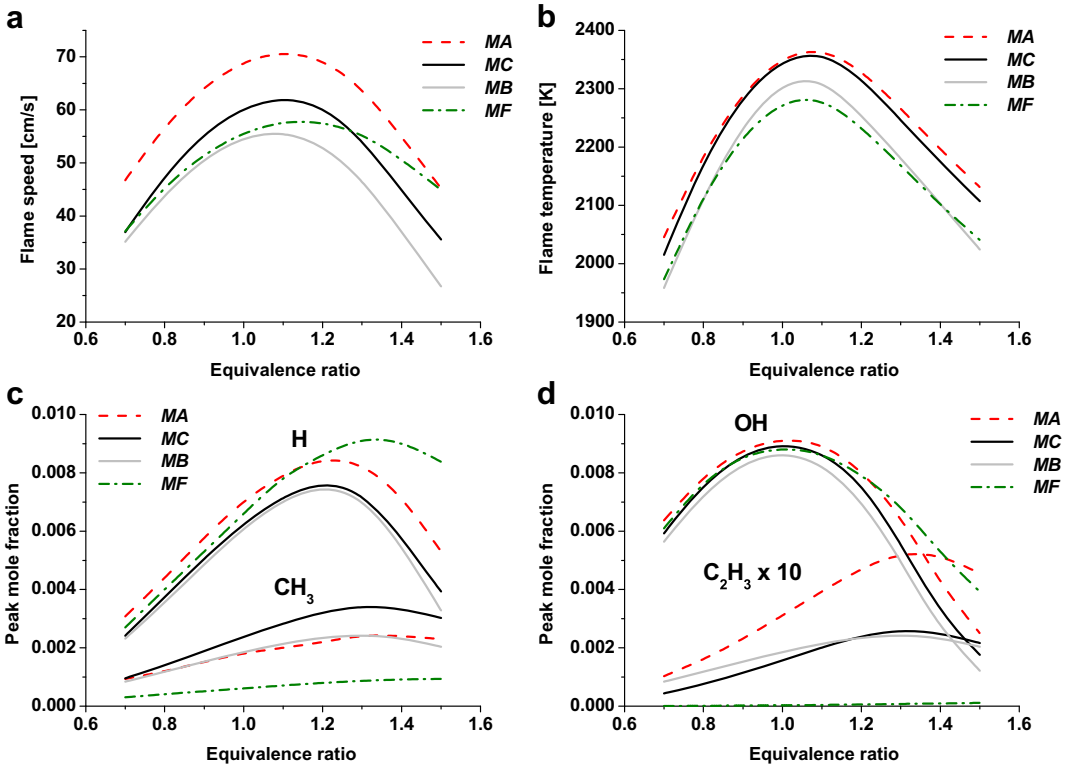

Fig. 17. Predicted laminar flame speeds of small methyl esters in air, at $T_0 = 403$ K and 1 atm. Panel a) Flame speeds; Panel b) Flame temperatures; Panel c) Peak mole fractions of H and CH_3 radicals; Panel d) peak mole fractions of OH and C_2H_3 radicals.

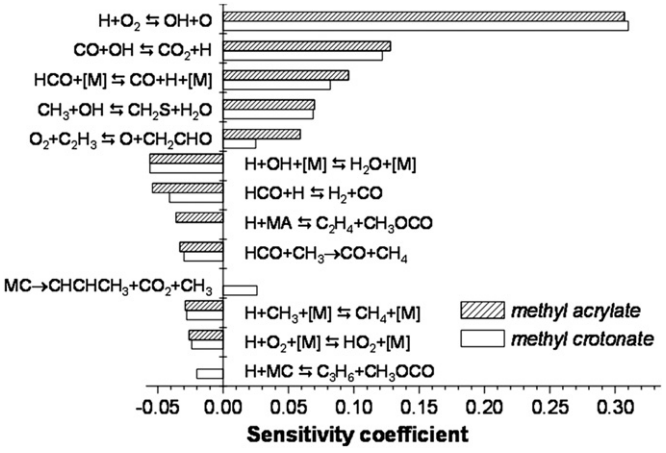

Fig. 18. Sensitivity coefficients of laminar flame speed on reaction rate coefficients, for methyl acrylate and methyl crotonate in air at $\Phi = 1$, $T = 403$ K and atmospheric pressure.

7. Conclusions

A semi-detailed kinetic model of methyl butanoate was proposed and validated. Because of the hierarchical approach, typical of the development of kinetic mechanisms, the work required the sequential building up and validation of the pyrolysis and oxidation mechanisms of methyl formate, methyl acrylate and methyl crotonate. This research activity made great use of previously developed kinetic models already available in the literature. The novelty and uniqueness of the proposed mechanism lies in its lumping formulation. The advantages of such an approach are quite clear and can be summarized quite simply.

A reduced number of species and reactions, proposed with analogy and similarity rules, facilitates the development of the kinetic scheme with an inherent control of rate constant consistency. The semi-detailed or lumped scheme allows the reduction of the computational effort and the direct use of the model in cases, such as laminar flames, where very detailed mechanisms cannot be adopted without a proper reduction. Finally, lumping models allow a more balanced description of primary and intermediate species, because they are treated with the same level of accuracy. Very detailed mechanisms, on the contrary, are often forced to describe the evolution of intermediate products in simplified ways, with an unbalanced description of the whole oxidation process.

The proposed model has been validated in comparison with a large set of experimental data, coming from different research groups and carried out in different operating conditions. This extensive activity gives general confidence in the mechanism and makes extrapolation to different conditions more reliable. The lumped scheme of methyl esters is included inside the whole combustion mechanism and will permit the direct analysis and description of complex mixtures of biodiesel and conventional transportation fuels. The advantage in terms of reduction of species and reactions of the lumped scheme for methyl butanoate is limited, however, due to the small methyl esters considered here. Nevertheless, the model and the approach proposed in this paper, together with the estimated rate constants, lay the foundation for an extension to methyl decanoate and heavier esters where the lumping description becomes a very useful opportunity in order to control the total number of involved species and reactions.

Acknowledgments

Authors gratefully acknowledge the useful work of Chiara Saggese and Giovanni Genova. This work has been partially supported by the 'Biodiesel project' of Istituto Motori CNR/MSE and by the EU as part of the COST Project CM0901.

Appendix

Low temperature reactions of methyl butanoate

Table A1 reports the low temperature reactions of methyl butanoate. These reaction subset is expected to be of limited importance, as already observed and discussed by Hakka et al. [27]. Following a well defined procedure discussed in Ranzi et al. [60], this mechanism refers to only four intermediate lumped radicals. Excluding the alkyl radical (RMBX) already involved in the high temperature mechanism of Table 1, we only consider one peroxy, one alkyl-hydroperoxy and one peroxy-alkyl-hydroperoxy radical with their oxidation and decomposition reactions.

Kinetic parameters of these lumped reactions are simply derived by fitting the initial selectivities obtained with the lumped reactions with the ones obtained with the detailed kinetic scheme reported by Hakka et al. [27], directly derived from EXGAS program. The fitting of kinetic parameters has been attained in the temperature range 650–1200 K and 1–25 atm. Fig. A1 shows the comparisons of the initial selectivities of the different reaction paths, as predicted by the detailed and lumped kinetic models. Namely the following products are considered: decomposition products (ethylene and propylene), methyl acrylate, cyclic-ethers with ketones, methyl crotonate and branching products. Apart from the three new radicals, only two new lumped molecular species are involved in the mechanism: one cyclic ether (ETMB: with the thermodynamic properties of the component C5H8O3E#3S of the Nancy database) and one lumped ketohydroperoxide (KEHYMB). The lumped cyclic ether also includes the ketone isomers. H-abstraction reactions are considered for the cyclic ether, while only a lumped initiation reaction is considered for KEHYMB. Thus the extension of the scheme to treat also the low temperature region only requires 5 new species and 12 reactions.

Table A1
Low temperature reactions of methyl butanoate. Lumped reactions are obtained by a simple fitting of Nancy mechanism [27].

	Reaction[a]	A	E_a
Methyl butanoate low temperature mechanism			
1	O_2 + RMBX → RMBOOX	3.5×10^8	0
2	RMBOOX → O_2 + RMBX	1.0×10^{13}	30,000[b]
3	RMBOOX → QMBOOX	1.5×10^{12}	25,000[b]
4	QMBOOX → RMBOOX	1.0×10^{10}	16,000
5	QMBOOX → HO_2 + MC	2.0×10^{11}	21,000
6	QMBOOX → OH + ETMB	1.5×10^{10}	11,500
7	O_2 + QMBOOX → ZMBOOX	3.5×10^8	0
8	ZMBOOX → O_2 + QMBOOX	2.0×10^{13}	30,000[b]
9	ZMBOOX → OH + KEHYMB	1.5×10^{12}	25,000[b]
10	KEHYMB → OH + CH_3CHO + CO + CH_3OCO	1.5×10^{16}	43,000
11	R + ETMB → RH + CO + CH_2O + C_2H_4CHO	$3H_{TIPO0}$	
12	R + ETMB → RH + C_2H_4 + CO + CO_2 + CH_3	$2H_{TIPO1}$	

RMBOOX = methyl butanoate peroxy radicals.
QMBOOX = methyl butanoate alkyl-hydroperoxy radicals.
ZMBOOX = methyl butanoate peroxy-alkyl-hydroperoxy radicals.
KEHYMB = methyl butanoate ketohydroperoxydes.
ETMB = methyl butanoate etherocycles.
[a] $k = A \exp(-E_a/RT)$. Units are: mole, l, s, K and cal.
[b] Activation energy has been modified. See text.

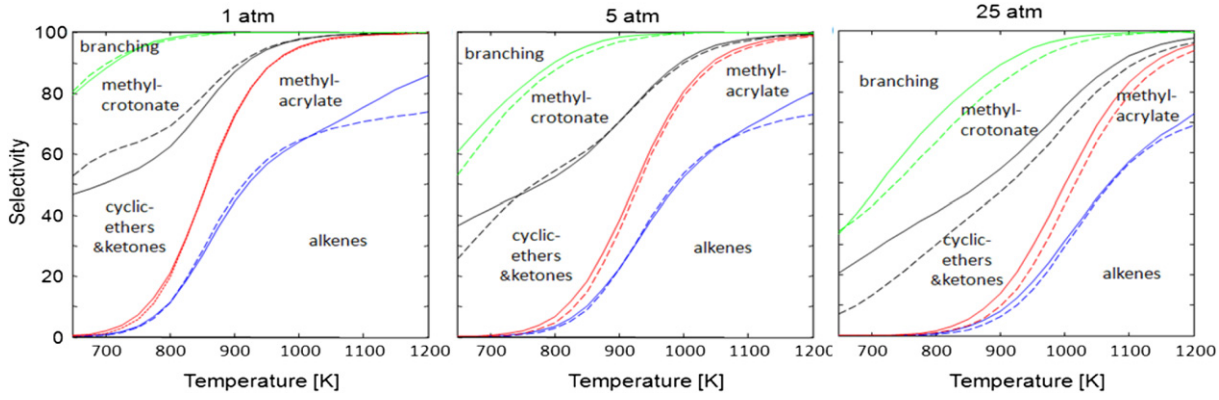

Fig. A1. Initial selectivities of major products from the oxidation of MB in air at 1, 5 and 25 atm. Comparisons between the predictions of the detailed (solid line) and the lumped (dashed lines) kinetic scheme.

The low temperature sub-mechanism is validated in comparison with the JSR experiments at 800 K [27], as well as with the autoignition delay times in the Lille RCM [61]. It is possible to verify that the effect of the LT mechanism is consistently higher and the predicted conversions are higher than the experimental ones for all the analyzed conditions. Furthermore, in the pressurized flow reactor at ~650 K in lean conditions ($\Phi = 0.35$, see Fig. 10), this lumped low temperature model predicts ~20% MB conversion, with 40 ppm of CH_2O, not experimentally measured.

For this reason, the importance of the lumped LT mechanism has been reduced. We simply increased the activation energy of peroxy radical isomerization from 25,000 kcal/mol to 26,000 kcal/mol and we reduced the activation energy of the decomposition reaction of peroxy radicals from 30,000 kcal/mol to 28,000 kcal/mol. Thus, Fig. A2 (Panel a) shows a comparison between JSR data and model predictions obtained both with the high temperature mechanism and with the complete mechanism including the modified low temperature reactions. The limited effect of the low temperature mechanism can be observed at low residence time, only at 800 K. Finally, Panel b) of the same figure shows a comparison of the ignition delay times in the RCM experiments at 815 K and $\Phi = 1$ in air. In these pressures conditions (10–20 atm), the LT mechanism allows to significantly reduce the ignition delay times from ~400 ms to less than 100 ms, in agreement with the experiments.

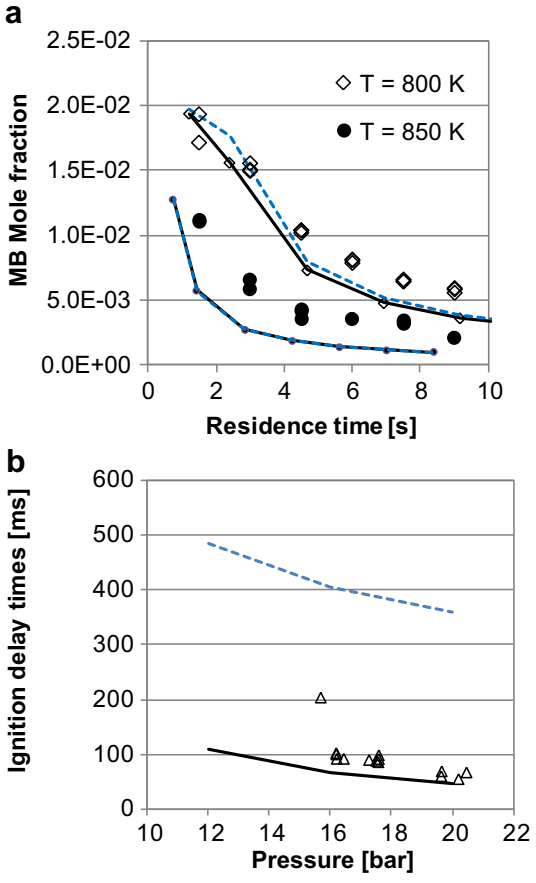

Fig. A2. Comparison of complete (solid lines) and high temperature (dashed lines) mechanisms of methyl butanoate. Panel a) conversion of methyl butanoate in the JSR [27]. Panel b) Ignition delay times in the RCM experiments at 815 K and $\Phi = 1$ in air [61].

References

[1] Herbinet O, Pitz WJ, Westbrook CK. Detailed chemical kinetic oxidation mechanism for a biodiesel surrogate. Combustion and Flame 2008;154:507–28.
[2] Knothe G. Biodiesel and renewable diesel: a comparison. Progress in Energy and Combustion Science 2010;36:364–73.
[3] Pitz WJ, Mueller CJ. Recent progress in the development of diesel surrogate fuels. Progress in Energy and Combustion Science 2011;37:330–50.
[4] Rashid U, Rehman HA, Hussain I, Ibrahim M, Haider MS. Muskmelon (Cucumis melo) seed oil: a potential non-food oil source for biodiesel production. Energy 2011;36(9):5632–9.
[5] Muralidharan K, Vasudevan D, Sheeba KN. Performance, emission and combustion characteristics of biodiesel fuelled variable compression ratio engine. Energy 2011;36(8):5385–93.
[6] Chen Y-H, Chen J-H, Luo Y-M, Shang N-C, Chang C-H, Chang C-Y, et al. 'Property modification of jatropha oil biodiesel by blending with other biodiesels or adding antioxidants. Energy 2011;36(7):4415–21.
[7] Satyanarayana M, Muraleedharan C. A comparative study of vegetable oil methyl esters (biodiesels). Energy 2011;36(4):2129–37.
[8] Haik Y, Selim MYE, Abdulrehman T. Combustion of algae oil methyl ester in an indirect injection diesel engine. Energy 2011;36(3):1827–35.
[9] Shuping Z, Yulong W, Mingde Y, Kaleem I, Chun L, Tong J. Production and characterization of bio-oil from hydrothermal liquefaction of microalgae Dunaliella tertiolecta cake. Energy 2010;35(12):5406–11.
[10] Sarin A, Arora R, Singh NP, Sarin R, Malhotra RK. Blends of biodiesels synthesized from non-edible and edible oils: Influence on the OS (oxidation stability). Energy 2010;35(8):3449–53.
[11] Sarin A, Arora R, Singh NP, Sarin R, Malhotra RK, Kundu K. Effect of blends of Palm-Jatropha-Pongamia biodiesels on cloud point and pour point. Energy 2009;34(11):2016–21.
[12] Tsolakis A, Megaritis A, Yap D. Application of exhaust gas fuel reforming in diesel and homogeneous charge compression ignition (HCCI) engines fuelled with biofuels. Energy 2008;33(3):462–70.
[13] Tsolakis A, Megaritis A, Wyszynski ML, Theinnoi K. Engine performance and emissions of a diesel engine operating on diesel-RME (rapeseed methyl ester) blends with EGR (exhaust gas recirculation). Energy 2007;32(11):2072–80.
[14] Fisher EM, Pitz WJ, Curran HJ, Westbrook CK. Detailed chemical kinetic mechanisms for combustion of oxygenated fuels. Symposium (International) on Combustion 2000;28:1579–86.
[15] El-Nahas AM, Navarro MV, Simmie JM, Bozzelli JW, Curran HJ, Dooley S, et al. Enthalpies of formation, bond dissociation energies and reaction paths for the decomposition of model biofuels: ethyl propanoate and methyl butanoate. Journal of Physical Chemistry A 2007;111:3727–39.
[16] Dooley S, Curran HJ, Simmie JM. Autoignition measurements and a validated kinetic model for the biodiesel surrogate, methyl butanoate. Combustion and Flame 2008;153:2–32.
[17] Metcalfe WK, Dooley S, Curran HJ, Simmie JM, El-Nahas AM, Navarro MV. Experimental and modeling study of $C_5H_{10}O_2$ ethyl and methyl esters. Journal of Physical Chemistry A 2007;111(19):4001–14.
[18] Metcalfe W, Simmie JM, Curran HJ. Ab initio chemical kinetics of methyl formate decomposition: the simplest model. Journal of Physical Chemistry A 2010;114:5478–84.
[19] Herbinet O, Pitz WJ, Westbrook CK. Detailed chemical kinetic mechanism for the oxidation of biodiesel fuels blend surrogate. Combustion and Flame 2010;157:893–908.
[20] Walton SM, Wooldridge MS, Westbrook CK. An experimental investigation of structural effects on the auto-ignition properties of two C5 esters. Proceedings of the Combustion Institute 2009;32(1):255–62.
[21] Westbrook CK, Pitz WJ, Westmoreland PR, Dryer FL, Chaos M, Osswald P, et al. A detailed chemical kinetic reaction mechanism for oxidation of four small alkyl esters in laminar premixed flames. Proceedings of the Combustion Institute 2009;32(1):221–8.
[22] Westbrook CK, Naik CV, Herbinet O, Pitz WJ, Mehl M, Sarathy SM, et al. Detailed chemical kinetic reaction mechanisms for soy and rapeseed biodiesel fuels. Combustion and Flame 2011;158:742–55.
[23] Battin-Leclerc F, Blurock E, Bounaceur R, Fournet R, Glaude P-A, Herbinet O, et al. Towards cleaner combustion engines through groundbreaking detailed chemical kinetic models. Chemical Society Reviews 2011;40(9):4762–82.
[24] Bax S, Hakka MH, Glaude P-A, Herbinet O, Battin-Leclerc F. Experimental study of the oxidation of methyl oleate in a jet-stirred reactor. Combustion and Flame 2010;157:1220–9.
[25] Glaude PA, Herbinet O, Bax S, Biet J, Warth V, Battin-Leclerc F. Modeling of the oxidation of methyl esters—Validation for methyl hexanoate, methyl heptanoate, and methyl decanoate in a jet-stirred reactor. Combustion and Flame 2010;157:2035–50.
[26] Hakka MH, Glaude P-A, Herbinet O, Battin-Leclerc F. Experimental study of the oxidation of large surrogates for diesel and biodiesel fuels. Combustion and Flame 2009;156:2129–44.
[27] Hakka MH, Bennadji H, Biet J, Yahyaoui M, Sirjean B, Warth V, et al. Oxidation of methyl and ethyl butanoates. International Journal of Chemical Kinetics 2010;42:226–52.
[28] Bennadij H, Coniglio L, Billaud F, Bounaceur R, Warth V, Glaude P-A, et al. Oxidation of small unsaturated methyl and ethyl esters. International Journal of Chemical Kinetics 2011;43(4):204–18.

[29] Herbinet O, Battin-Leclerc F, Bax S, LeGall H, Glaude P-A, Fournet R, et al. Detailed product analysis during the low temperature oxidation of n-butane. Physical Chemistry Chemical Physics 2011;13:296–308.
[30] Herbinet O, Biet J, Hakka MH, Warth V, Glaude P-A, Nicolle A, et al. Modeling study of the low-temperature oxidation of large methyl esters from C11 to C19. Proceedings of the Combustion Institute 2011;33:391–8.
[31] Herbinet O, Glaude PA, Warth V, Battin-Leclerc F. Experimental and modeling study of the thermal decomposition of methyl decanoate. Combustion and Flame 2011;158:1288–300.
[32] Dagaut P, Gaïl S, Sahasrabudhe M. Rapeseed oil methyl ester oxidation over extended ranges of pressure, temperature, and equivalence ratio: experimental and modeling kinetic study. Proceedings of the Combustion Institute 2007;31:2955–61.
[33] Dayma G, Gaïl S, Dagaut P. Experimental and kinetic modeling study of the oxidation of methyl hexanoate. Energy and Fuels 2008;22:1469–79.
[34] Dayma G, Togbè C, Dagaut P. Detailed kinetic mechanism for the oxidation of vegetable oil methyl esters: new evidence from methyl heptanoate. Energy and Fuels 2009;23:4254–68.
[35] Gaïl S, Thomson MJ, Sarathy SM, Syed SA, Dagaut P, Diévart P, et al. A wide-ranging kinetic modeling study of methyl butanoate combustion. Proceedings of the Combustion Institute 2007;31:305–11.
[36] Gaïl S, Sarathy SM, Thomson MJ, Diévart P, Dagaut P. Experimental and chemical kinetic modeling study of small methyl esters oxidation: methyl (E)-2-butenoate and methyl butanoate. Combustion and Flame 2008;155:635–50.
[37] Sarathy SM, Gaïl S, Syed SA, Thomson MJ, Dagaut P. A comparison of saturated and unsaturated C4 fatty acid methyl esters in an opposed flow diffusion flame and a jet stirred reactor. Proceedings of the Combustion Institute 2007;31:1015–22.
[38] Togbè C, May-Carle J-B, Dayma G, Dagaut P. Chemical kinetic study of the oxidation of a biodiesel-Bioethanol surrogate fuel: methyl octanoate-ethanol mixtures. Journal of Physical Chemistry A 2010;114:3896–908.
[39] Togbè C, Dayma G, Mze-Ahmed A, Dagaut P, Experimental, Modeling. Study of the kinetics of oxidation of simple biodiesel-biobutanol surrogates: methyl octanoate-butanol mixtures. Energy and Fuels 2010;24:3906–16.
[40] Marchese AJ, Angioletti M, Dryer FL. Symposium (International) on Combustion 2004, Work in progress poster 1F1-03.
[41] Dooley S, Burke MP, Chaos M, Stein Y, Dryer FL, Zhukov VP, et al. Methyl formate oxidation: speciation data, laminar burning velocities, ignition delay times, and a validated chemical kinetic model. International Journal of Chemical Kinetics 2010;42:527–9.
[42] Dooley S, Dryer FL, Yang B, Wang J, Cool TA, Kasper T, et al. An experimental and kinetic modeling study of methyl formate low-pressure flames. Combustion and Flame 2011;158:732–41.
[43] Lu TF, Law CK. Toward accommodating realistic fuel chemistry in large-scale computations. Progress in Energy and Combustion Science 2009;35:192–215.
[44] Seshadri K, Lu T, Herbinet O, Humer S, Niemann U, Pitz WJ, et al. Experimental and kinetic modeling study of extinction and ignition of methyl decanoate in laminar non-premixed flows. Proceedings of the Combustion Institute 2009;32:1067–74.
[45] Luo Z, Lu T, Maciaszek MJ, Som S, Longman DE. A reduced mechanism for high-temperature oxidation of biodiesel surrogates. Energy and Fuels 2010;24:6283–93.
[46] Dente M, Pierucci S, Ranzi E, Bussani G. New improvements in modelling kinetic schemes for hydrocarbon pyrolysis reactors. Chemical Engineering Science 1992;47:2629–36.
[47] Ranzi E, Dente M, Bozzano G, Goldaniga A, Faravelli T. Lumping procedures in detailed kinetic models of gasification, pyrolysis, partial oxidation and combustion of hydrocarbon mixtures. Progress in Energy and Combustion Science 2001;27:99–139.
[48] Ranzi E, Faravelli T, Frassoldati A, Granata S. Wide-range kinetic modeling study of the pyrolysis, partial oxidation, and combustion of heavy n-alkanes. Industrial and Engineering Chemistry Research 2005;44:5170–83.
[49] Ranzi E. A wide range kinetic modeling study of oxidation and combustion of transportation fuels and surrogate mixtures. Energy and Fuels 2006;20:1024–32.
[50] Good DA, Francisco JS. Tropospheric oxidation mechanism of dimethyl ether and methyl formate. Journal of Physical Chemistry A 2000;104:1171–85.
[51] Ranzi E, Dente M, Faravelli T, Pennati G. Prediction of kinetic parameters for H-Abstraction Reactions. Combustion Science and Technology 1994;95:1–50.
[52] Zhao Z, Chaos M, Kazakov A, Dryer FL. Thermal decomposition reaction and a comprehensive kinetic model of dimethyl ether. International Journal of Chemical Kinetics 2008;10:1–18.
[53] Farooq A, Davidson DF, Hanson RK, Huynh LK, Violi A. An experimental and computational study of methyl ester decomposition pathways using shock tubes. Proceedings of the Combustion Institute 2009;32(1):247–53.
[54] Huynh LK, Violi A. Thermal decomposition of methyl butanoate: ab initio study of a biodiesel fuel surrogate. Journal of Organic Chemistry 2008;73:94–101.
[55] Huynh LK, Lin KC, Violi A. Kinetic modeling of methyl butanoate in shock tube. Journal of Physical Chemistry A 2008;112(51):13470–80.
[56] Veloo PS, Wang YL, Egolfopoulos FN, Westbrook CK. A comparative experimental and computational study of methanol, ethanol, and n-butanol flames. Combustion and Flame 2010;157:1989–2004.
[57] Wang YL, Feng Q, Egolfopoulos FN, Tsotsis TT. Studies of C4 and C10 methyl ester flames. Combustion and Flame 2011;158:1507–19.
[58] Liu W, Kelley AP, Law CK. Non-premixed ignition, laminar flame propagation and mechanism reduction of n-butanol, iso-butanol and methyl butanoate. Proceedings of the Combustion Institute 2011;33:995–1002.
[59] [Chapter 7] Law CK. Laminar premixed flames. In: Combustion physics. New York: Cambridge University Press; 2006.
[60] Ranzi E, Faravelli T, Gaffuri P, Pennati G. Low Temperature combustion: automatic generation of primary oxidation reactions and lumping procedures. Combustion and Flame 1995;102:179–92.
[61] HadjAli K, Crochet M, Vanhove G, Ribaucour M, Minetti R. A study of the low temperature autoignition of methyl esters. Proceedings of the Combustion Institute 2009;32:239–46.